

# CO<sub>2</sub> storage at the Atzbach–Schwanenstadt gas field: a seismic monitoring feasibility study

Giuliana Rossi,<sup>1\*</sup> Davide Gei,<sup>1</sup> Stefano Picotti,<sup>1</sup> and José M. Carcione<sup>1</sup>

**G**eological storage of carbon dioxide (CO<sub>2</sub>), i.e. its injection in the subsurface is one of the options to reduce the emission of probably the most harmful greenhouse gas. When stored into existing oil and gas fields or unmineable coal seams, the CO<sub>2</sub> injected has additional economic benefits through enhanced oil/gas recovery (EOR/EGR) or coal-bed methane production (e.g. Baines and Worden, 2004). While EOR is a well established technology, the possibility of EGR, due to the pushing effect of the CO<sub>2</sub> cushion, is not yet proven notwithstanding several studies on the topic (e.g. Oldenburg, 2003; Oldenburg et al. 2004).

Injection is already active in the gas-fields K12-B, offshore The Netherlands, while other sites in Japan, US, Australia, and Europe are object of feasibility and pre-injection studies (e.g. Riddiford et al., 2004; Kreft et al., 2006). Among these, the Atzbach-Schwanenstadt gas field is one of the four test sites of the EU co-funded CASTOR (CO<sub>2</sub> from CAPture to STORAge) project to test and validate the technology. The Atzbach-Schwanenstadt almost depleted gas field is located in central northern Austria (Figure 1), in the Molasse Basin in the foreland of the Alpine mountain chain, outside the area affected by compressional deformation. The reservoir sandstone intervals, approximately 1600 m below the surface, were formed in the Puchkirchen Basin, a deep-water trough parallel to the alpine front.

Rohoel is considering its transformation into a CO<sub>2</sub> storage site and is testing the suitability of CO<sub>2</sub> injection for EGR. Potential CO<sub>2</sub> sources are a paper mill (emitting about 200000 tonnes CO<sub>2</sub> per year) and a fertilizer plant (emitting about 100000 tonnes CO<sub>2</sub> per year), while the transport of

CO<sub>2</sub> may be done by trucks. Geophysics, geochemistry, geo-mechanics, and reservoir engineering are the disciplines to investigate within the CASTOR project the possibility of Enhanced Gas Recovery as well as the effect of CO<sub>2</sub> injection on the mechanical stability of the site. Moreover, the studies estimate the risk for CO<sub>2</sub> migration to the groundwater or the atmosphere (Polak et al., 2006). A key point, particularly when the site is onshore, is to provide confidence in predictions of the long-term fate of CO<sub>2</sub> in the subsurface and to identify and measure any potentially hazardous leaks to the surface, requiring an efficient monitoring program of the stored CO<sub>2</sub>.

The choice among the wide range of monitoring tools available depends on the site characteristics, the objective and the costs (e.g. Benson et al., 2004; Arts and Winthagen, 2005). Normally, 3D surface seismic, eventually complemented by multi-component seismic surveys, cross-hole seismics, and VSP would be the main tool for controlling the CO<sub>2</sub> fate during the pre-injection, injection, and post-injection phases, as demonstrated in the Sleipner field (e.g. Arts et al., 2004). In this particular case, however, due to the presence of residual methane, the conditions for seismics to map the CO<sub>2</sub> plume are less favourable than for a depleted oil reservoir or saline aquifer. In general, the sensitivity of the time-lapse (4D) seismic survey in detecting variations in fluid saturation, depends i) upon the geological characteristics of the reservoir and the overburden, and ii) upon the seismic parameters that will be adopted for the experiment. Seismic modelling is a suitable tool to image specific geological settings and to simulate different CO<sub>2</sub> sequestration scenarios, but its success depends on a correct description of the physical properties of the CO<sub>2</sub> bearing rocks. The present work investigates the sensitivity of the seismic properties to small variations in CO<sub>2</sub> and in CH<sub>4</sub> within the reservoir, as a feasibility study for future seismic time-lapse surveys.

## Integrated seismic modelling method

Figure 2 shows a scheme of our integrated method for seismic monitoring evaluation and planning. Studies of the rock and fluid physical properties constitute the basis to understand the sensitivity of seismic properties to small variations



Figure 1 Location of the gas-field of Atzbach-Schwanenstadt.

<sup>1</sup> Istituto Nazionale di Oceanografia e di Geofisica (OGS), Borgo Grotta Gigante 42/C, Sgonico 34010, Italy.

\*Corresponding author: Giuliana Rossi, E-mail: grossi@inogs.it.

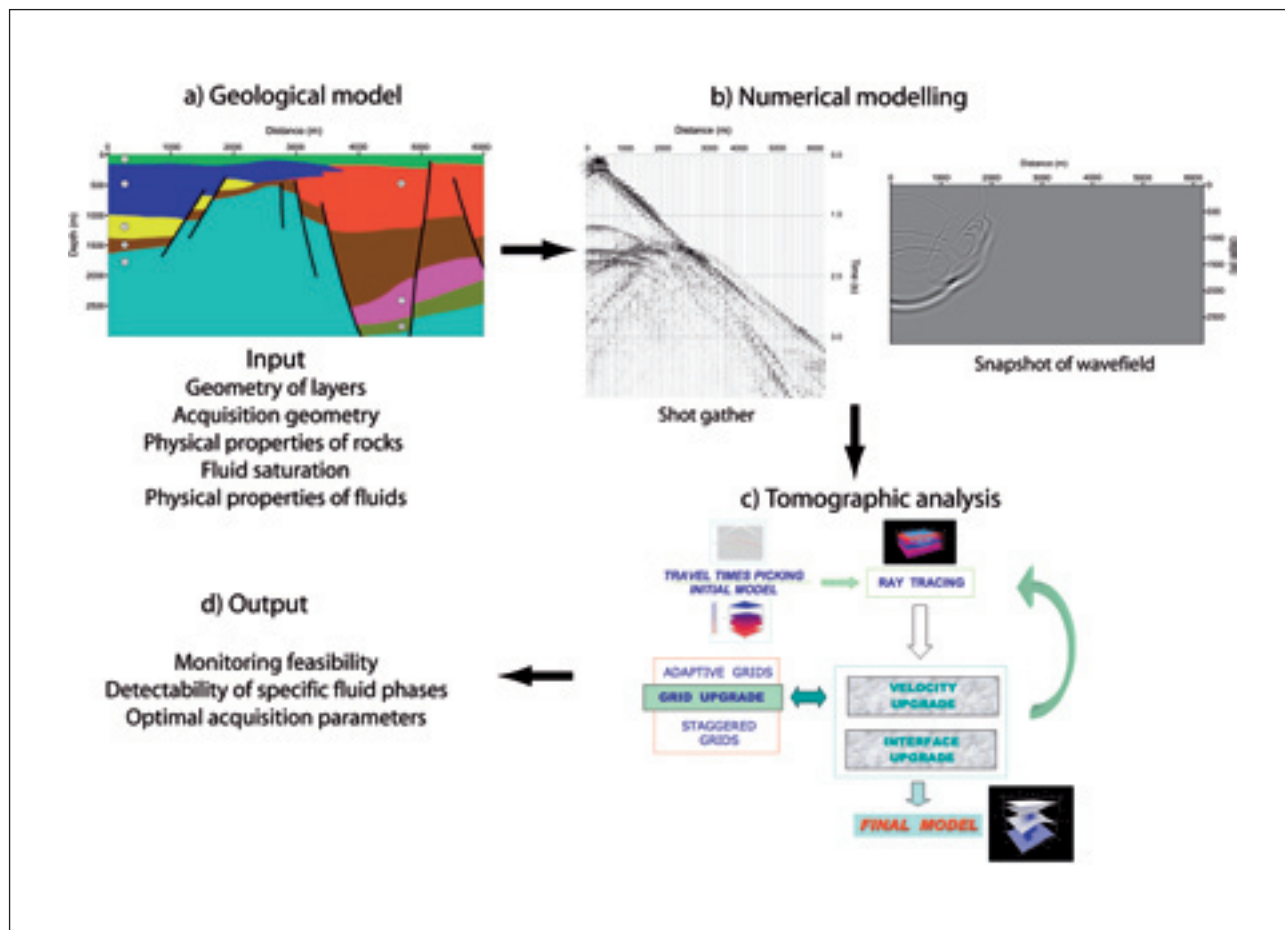
CO<sub>2</sub> Sequestration

Figure 2 Integrated method, including theoretical studies on seismic properties of rocks and fluids, numerical modelling, tomographic forward and inverse modelling.

in the fluid content within the rock. Moreover, the physical properties of the rocks are used in the numerical modelling to compute the synthetic seismograms. Tomographic analysis of the synthetic data enables us to test the feasibility of monitoring a CO<sub>2</sub> storage site and tune the optimal acquisition parameters.

The models to obtain the seismic properties are based on a poro-viscoelastic theory for shaly sandstones. The poro-viscoelastic equations, which constitute the kernel of the modelling algorithm, are solved using a fourth-order Runge-Kutta time-stepping scheme and the staggered Fourier method for computing the spatial derivatives. The input parameters are mainly the porosity, saturation, viscosity, dry-rock moduli, clay content, quality factors, temperature, pore pressure, and confining stress. The differential equations of motion are given and the approach generalizes the Gassmann modulus commonly used for fluid substitution. The modelling provides the full wave field for arbitrary geometries of the layers and general material properties (Carcione and Helle, 1999; Carcione et al., 2003a, b).

Our proprietary tomographic package CAT-3D enables forward and inverse problems to be approached. P- and S-wave velocity fields may be computed as well as the geometry of the reflectors. The software includes integrated tools for an accurate estimation of the reliability of the tomographic system and for the quality control of the results. The software enables joint use of different kinds of waves (reflected, refracted, direct, and converted) (Böhm et al., 1999). Moreover, the combined use of irregular grids and of the grid staggering method produces high resolution velocity-field images, without losing the robustness of the inversion (Vesnaver et al., 1999; Vesnaver and Böhm, 2000). Frequency shift tomography is associated to the more common travel-times tomography to provide an attenuation model in addition to the seismic velocity (e.g. Rossi et al., 2007).

### Acoustic properties of the fluids

In order to model the seismic response on a storage site, it is necessary to calculate the physical properties of the dif-

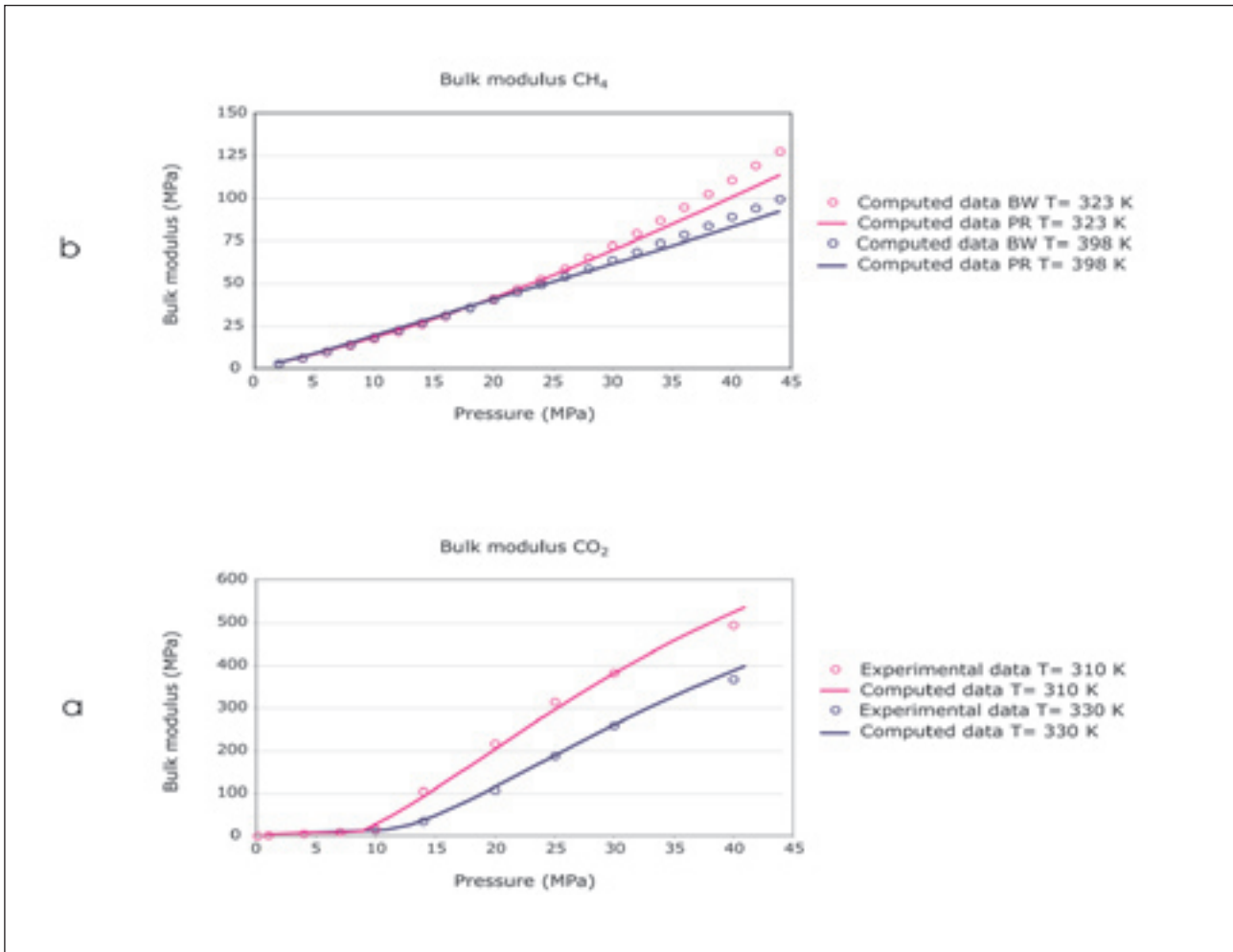


Figure 3 – a) Comparison of experimental and computed bulk modulus for carbon dioxide (experimental data from Wangand Nur (1989)). b) Comparison of bulk modulus of methane computed with the Peng-Robinson Equations of state (PR) and with Batzle and Wang (1992) semi-empirical formulas (BW).

ferent fluids (brine, oil, natural gas, and carbon dioxide), to simulate the different scenarios of the injection process (e.g. Carcione et al., 2006). The most common method used to compute the density of pure components or mixtures of fluids at supercritical conditions, such as carbon dioxide, is the use of equations of state (EoS). We consider the Peng-Robinson EoS (Peng and Robinson, 1976), a cubic equation derived from the van der Waals equation of state. Isothermal compressibility  $c_T$  of gases can be obtained from the EoS considering the formula  $c_T = -1/V (\partial V / \partial P)$  where  $V$  is volume and  $P$  is pressure (Morse and Ingard, 1986). The bulk modulus of the gas  $K_G$  is defined as the inverse of the adiabatic compressibility  $c_S$ , which is related to the isothermal compressibility  $c_T$  through the specific heat ratio

$$\gamma: c_S = c_T / \gamma. \text{ Hence, } K_G \text{ is given by: } K_G = \gamma V \left( \frac{\partial P}{\partial V} \right).$$

The specific heat ratio for methane is given by Batzle and Wang (1992). We obtained the specific heat ratio for CO<sub>2</sub>

from regression of experimental data. The viscosity of pure gas components and gas mixtures, as a function of pressure and temperature, is determined using the Lohrenz-Bray-Clark theory (Lohrenz et al., 1964). This model uses the concept of residual viscosity, which is defined as the difference between viscosity at prevailing conditions and at low pressure, where the viscosity depends only on the thermal energy. It can be related to the fluid density, whereas the viscosity of gases at low pressure can be determined by the kinetic theory of gases.

The brine acoustic properties depend on temperature, pressure, and salinity. Batzle and Wang (1992) provide a series of useful empirical relations between the state variables and velocity and density. Viscosity of brine can be computed as a function of water salinity and temperature (Batzle and Wang, 1992). The equations are limited to the pressures and temperatures of the experiments (around 60 MPa and 100 °C) made by Batzle and Wang (1992). Figure 3 shows the comparison between the bulk modulus of car-

# CO<sub>2</sub> Sequestration

bon dioxide and methane respectively, calculated with different formulas and compared with the experimental data (when available).

## Atzbach-Schwanenstadt physical model

The geological model has been built on the basis of seismic interpretation, geological knowledge, and well log data (Polak et al., 2006), including the topographic surface and one low velocity layer to simulate the weathering (Figure 4).

The model was then populated with the physical properties provided in part by the partners and in part from the existing literature, whereas the fluid properties were calculated as described above. Table 1 shows the different layers, their geological composition, pressure and temperature conditions, and the physical properties for different

fluid saturations. The CO<sub>2</sub> is supposed to be injected in the A4 formation, a shaly sandstone within the sedimentary sequence (layer 5 in our model). We calculated different percentages of methane and respectively carbon dioxide, in order to evaluate the sensitivity of the seismic properties, as the wave velocity, to small variations of the percentages: the relative values are indicated in correspondence of the rows of layer 5.1 (brine +CH<sub>4</sub>) and 5.2 (brine + 50% CO<sub>2</sub> and 50%CH<sub>4</sub>) etc.. We calculated the physical properties in case of CO<sub>2</sub> migrating in one of shallower layers, for example through an abandoned well: the resulting properties are in the rows 1.2 and 4.1.

As expected, the change in seismic properties is noticeable when there is injection of the gas mixture in a layer containing only brine, whereas the variation is much small-

Formation	Average depth (m)	Pressure (MPa)	Temperature (°C)	Solid material	Saturating fluid	Sw	Cc	ρs (kg/m3)	Ks (GPa)	φ	Km (GPa)	μm (GPa)
0 Overburden	106	1.37	37.7	clay+sand	brine+air	0.3	0.5	2625	24.3	0.30	6.81	0.31
1 HSHT	590	6.06	29.8	clay+sand	brine	1.0	0.3	2635	29.2	0.26	7.80	3.75
1.1 HSHT	590	6.06	29.8	clay+sand	brine+CH4	0.4	0.3	2635	29.2	0.26	7.80	3.75
1.2 HSHT - leakage	900	9.20	37.5	clay+sand	brine+CO2+CH4	0.4	0.3	2635	29.2	0.26	7.80	3.75
2 Hall (HS_base)	1088	11.30	42.2	clay+sand	brine	1.0	0.7	2825	19.1	0.20	10.38	4.79
3 A2 (A2_top)	1220	13.12	42.2	clay+sand	brine	1.0	0.8	2822	18.9	0.15	10.81	4.56
4 A3 (A4_top)	1588	16.15	54.7	clay+sand	brine	1.0	0.5	2825	24.3	0.17	14.43	7.90
4.1 A3 (A4_top) - leakage	1088	11.30	54.7	clay+sand	brine+CO2(50%)+CH4(10%)	0.5	0.5	2825	24.3	0.17	14.43	7.90
5.0 A4 (A4_base)	1788	18.17	59.7	clay+sand	brine	1.0	0.3	2825	29.2	0.17	10.70	10.58
5.1 A4 (A4_base)	1788	18.17	59.7	clay+sand	brine+CH4(10%)	0.4	0.3	2825	29.2	0.17	10.70	10.58
5.2 A4 (A4_base)	1788	18.17	59.7	clay+sand	brine+CO2(50%)+CH4(50%)	0.4	0.3	2825	29.2	0.17	10.70	10.58
5.3 A4 (A4_base)	1788	18.17	59.7	clay+sand	brine+CO2(90%)+CH4(10%)	0.4	0.3	2825	29.2	0.17	10.70	10.58
5.4 A4 (A4_base)	1788	18.17	59.7	clay+sand	brine+CO2(100%)	0.4	0.3	2825	29.2	0.17	10.70	10.58
6 Channel	1888	18.18	62.2	clay+sand	brine	1.0	0.4	2822	28.8	0.15	10.70	11.05
7 SST (Top Forane)	1988	20.15	64.7	clay+sand	brine	1.0	0.5	2825	24.3	0.15	9.63	7.38
8 Forane	2288	23.22	72.2	infrasilite	brine	1.0	0.5	2882	57.2	0.15	42.41	22.06

ρm	T	ηf (cP)	κ (mD)	ρf (kg/m³)	Kf (GPa)	Q	Vp (km/s)	Vs (km/s)	Vp/Vs	ρ (kg/m³)	Acoustic impedance contrast	Ksat (GPa)	μsat (GPa)	Csat
0.33	1.17	0.006	40.00	319.84	0.00	5.90	800	400	2.00	1923	0.475	0.82	0.31	0.33
0.34	1.42	0.005	40.00	1032.59	2.54	72.76	2600	1300	2.00	2218	0.532	9.99	3.75	0.33
0.34	1.42	0.019	40.00	494.80	0.02	46.50	2078	1046	1.94	2071	0.272	3.95	3.75	0.34
0.34	1.42	0.092	40.00	501.16	0.02	46.28	2072	1041	1.95	2085	0.302	3.97	3.75	0.34
0.38	1.00	0.750	112.80	1030.06	2.83	115.92	3276	1628	2.02	2299	-0.020	10.41	4.69	0.38
0.37	1.82	0.004	14.96	1029.02	2.86	99.67	3642	1886	2.19	2372	0.950	15.93	4.56	0.37
0.27	1.44	0.832	33.50	1027.19	2.70	125.09	3409	1820	1.86	2352	0.928	16.82	7.90	0.20
0.27	1.44	0.089	33.50	776.35	0.09	117.81	3305	1689	1.79	2311	0.929	14.71	7.90	0.27
0.24	1.44	0.090	24.50	1025.72	2.72	152.04	3750	2116	1.78	2381	0.929	17.23	10.58	0.27
0.24	1.44	0.082	24.50	519.52	0.06	145.93	3662	2156	1.71	2325	0.934	16.74	10.58	0.24
0.24	1.44	0.104	24.50	607.67	0.07	145.07	3671	2149	1.71	2350	0.932	16.79	10.58	0.24
0.24	1.44	0.138	24.50	757.68	0.11	143.63	3653	2137	1.71	2316	0.929	16.80	10.58	0.24
0.24	1.44	0.153	24.50	820.02	0.14	143.09	3646	2132	1.71	2326	0.928	16.82	10.58	0.24
0.23	1.83	0.571	14.96	1024.95	2.7	151.53	3752	2150	1.74	2389	-0.080	18.93	11.05	0.26
0.19	1.83	0.553	14.96	1024.13	2.7	110.22	3200	1799	1.82	2385	0.256	14.58	7.38	0.28
0.28	1.83	0.592	14.96	1021.49	2.7	291.06	5200	2850	1.82	2700		43.63	22.06	0.28

S <sub>w</sub>	water saturation (%)
C <sub>c</sub>	(dry content (%))
ρ <sub>s</sub> (kg/m <sup>3</sup> )	density of the solid grains (e.g. a mixture of Quartz and Clay)
K <sub>s</sub> (GPa)	bulk modulus of the material forming the solid grains
φ	porosity
K <sub>m</sub> (GPa)	bulk modulus of the solid frame (dry rock bulk modulus)
μ <sub>m</sub> (GPa)	shear modulus of the solid frame (dry rock shear modulus)
σ <sub>v</sub>	Poisson's ratio of the solid frame
T	torquosity
η <sub>f</sub> (cP)	fluid viscosity (e.g. viscosity of liquid-gas mixture)
κ (mD)	permeability
ρ <sub>f</sub> (kg/m <sup>3</sup> )	fluid phase density (e.g. density of liquid-gas mixture)
K <sub>f</sub> (GPa)	fluid phase bulk modulus (e.g. bulk modulus of liquid-gas mixture)
Q	quality factor
V <sub>p</sub> (km/s)	P-wave velocity
V <sub>s</sub> (km/s)	S-wave velocity
ρ (kg/m <sup>3</sup> )	bulk density
K <sub>sat</sub> (GPa)	bulk modulus of the wet rock
μ <sub>sat</sub> (GPa)	shear modulus of the wet rock
σ <sub>v</sub>	Poisson's ratio of the wet rock

Table 1 The characteristics and physical properties for the different formations, from literature, theory and partner communication. Here above the symbol explanation.

er in the presence of methane, since the physical properties are very similar. It is worth noticing how the change in CO<sub>2</sub> percentage from 50% to 90% causes a decrease in seismic P-wave velocity of only about 20 m/s, while density drops with 26 kg/m<sup>3</sup>, and consequently the acoustic impedance varies by 0.3 %. There is also a slight variations in the quality factor (Q) of the P waves, and therefore in the amplitude and frequency of the seismic pulses. This means that the variations to be expected in a seismic experiment are really subtle, if the aim is to quantify variation in fluid concentration within the reservoir.

**Simulating a seismic acquisition and inversion**

We simulated a seismic line shot along a 2D section coinciding with one of the migrated seismic sections available (Figure 5). The staggered grid, corresponding to the geological model above, has 800 x 720 points, and the source is a Ricker wavelet with a dominant frequency of 20 Hz. Use of the described methodology allows us to have a direct control of the reservoir properties, such as, dry rock moduli, porosity, permeability, and fluid properties, and in situ conditions such as pore pressure and temperature. We computed the synthetic data before CO<sub>2</sub> injection (methane + brine in the reservoir with a gas saturation of 66 %) and after injection (methane + carbon dioxide + brine in the reservoir; gas saturation is 66 % and the CO<sub>2</sub> volume fraction with respect to CH<sub>4</sub> is 90%). The poro-viscoelastic seismograms before and after CO<sub>2</sub> injection show the expected differences (Figure 6). The leakage that we hypothesized corresponding to an abandoned well above the reservoir is easily identifiable. Discrimination between methane and carbon dioxide in the reservoir is possible on synthetic data. Nevertheless, the differences are subtle, and they may be masked in presence of noise, or non-repeatable acquisition patterns.

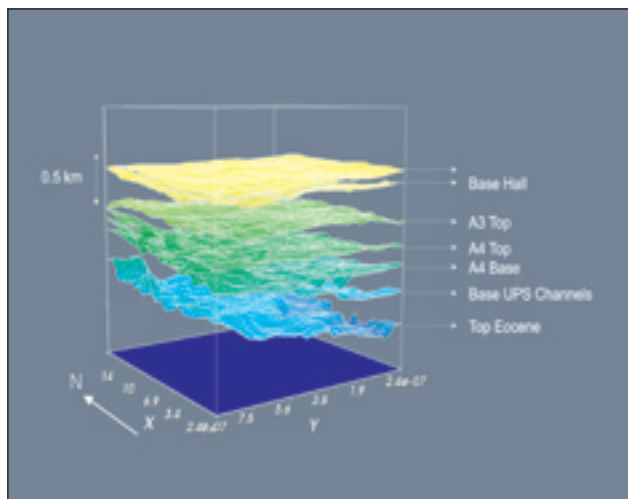


Figure 4 Atzbach-Schwanenstadt geological model: the colours are relative to the interface depth.

A common procedure, when assessing the similarity of two time-lapse data sets, is to use repeatability metrics, such as the normalized rms (NRMS), where

$$NRMS = 100 \frac{RMS(repeat - base)}{0.5(RMS(repeat) + RMS(base))} \text{ (e.g. Kragh and Christie, 2002).}$$

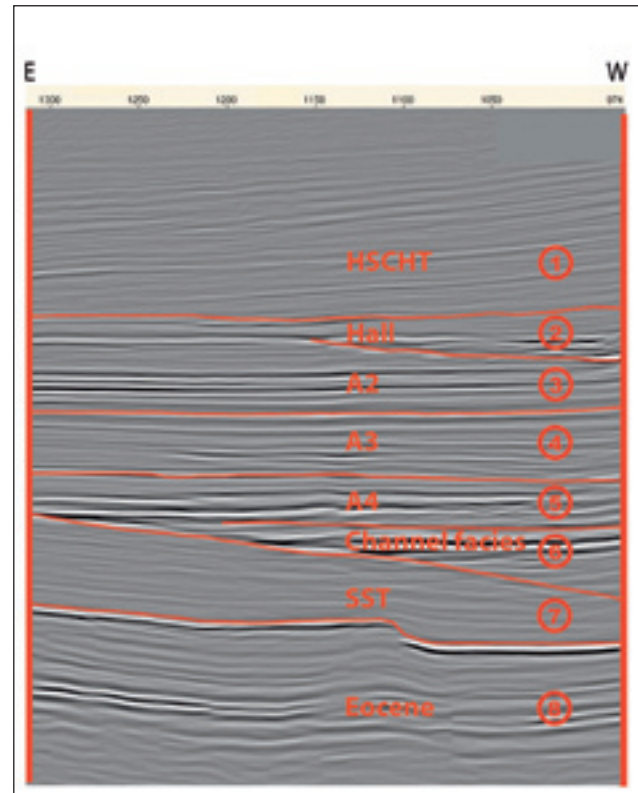


Figure 5 Seismic section relative to the geological model. The geological interpretation is superimposed. Each formation is identified by a number to help the identification in the table of properties.

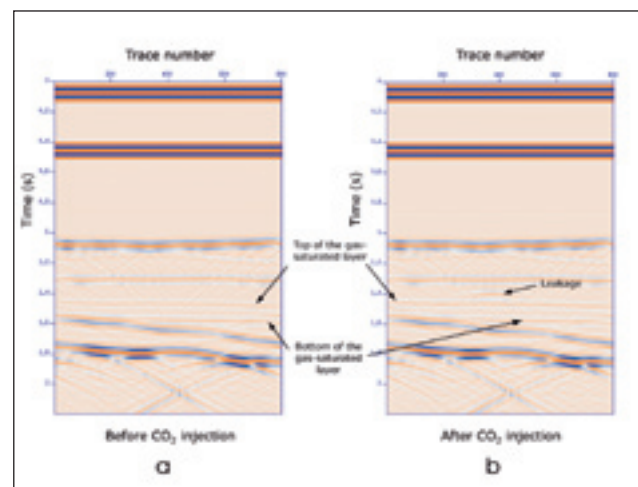


Figure 6 a) Synthetic seismic section (near trace) correspondent to the original one of Figure 5. before CO<sub>2</sub> injection; b) after CO<sub>2</sub> has been injected. A leakage in the A3 formation above the reservoir along an abandoned well is simulated (1-1.2 s).

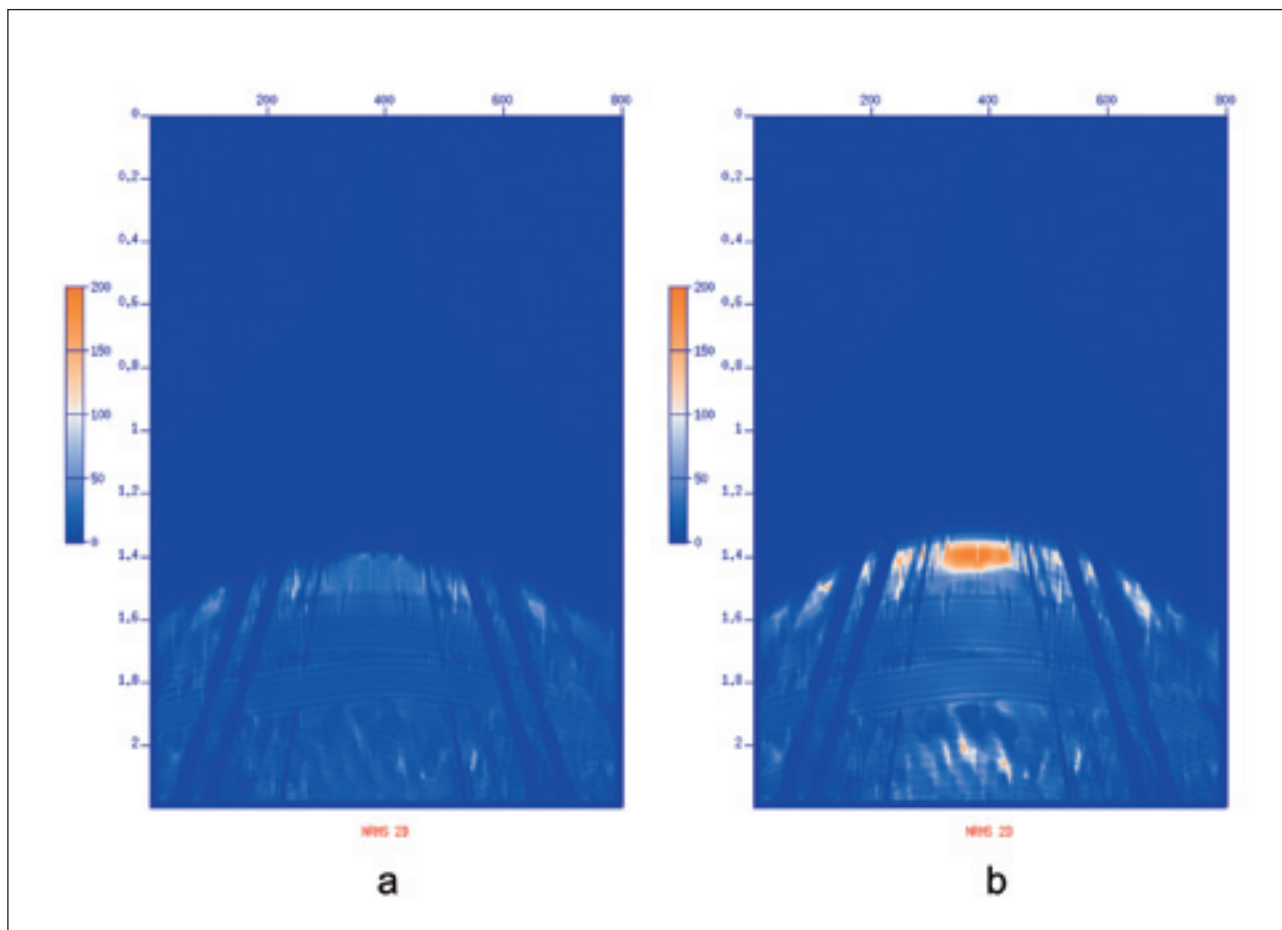
CO<sub>2</sub> Sequestration

Figure 7 NRMS sections for a) 50% CO<sub>2</sub> and 50% CH<sub>4</sub> in the reservoir; b) 90% CO<sub>2</sub> and 10% CH<sub>4</sub>; c) 90% CO<sub>2</sub> and 10% CH<sub>4</sub> plus leakage of the same mixture in the A3 formation above.

In Figure 7 the comparison between three shots: a) the NRMS in the case of 90% CO<sub>2</sub> and 10% CH<sub>4</sub>, and c) the same but in the presence of leakage in the A3 formation. The difference is above the 15% that has been measured in real seismic data (Kragh and Christie, 2002). Therefore, notwithstanding the difficulties of the repeatability of a seismic survey onshore, possible CO<sub>2</sub> migration should be detectable.

### Conclusions

For the difficult case presented in this paper, i.e. a gas-reservoir on-shore, time-lapse seismic technology is able to detect the possible migration above the reservoir when escaping, for example, through a leaking abandoned well. Regarding the mapping of the CO<sub>2</sub> plume, i.e. the detection of gas concentration variations, the sensitivity of the surface seismic survey is low, but not negligible. Adding downhole sensors in the wells and integration with other surface and borehole measurements, e.g. gravity (Sherlock et al., 2006), may improve the tracking of the CO<sub>2</sub> plume in the reservoir.

### Acknowledgments

The work is part of the EU funded CASTOR project. We are indebted to the WP3.2 partners for helpful discussions, data exchange, and suggestions. We would like to thank Rohoel AG for their cooperation and support, and permission to present these results. Finally, we thank Rob Art for reviewing the manuscript and the fruitful comments.

### References

- Arts, R. and Winthagen, P. [2005]. In: Benson, S. (Ed.). *Carbon Dioxide Capture for Storage in Deep Geologic Formations – Results from the CO2 Capture Project: Vol. 2*, Elsevier Oxford, 1001-1013.
- Arts, R., Eiken, O., Chadwick, A., Zweigel, P., Van der Meer, B., and Kirby, G. [2004] In: Baines S and Worden R.H. (Eds). *Geological storage of carbon dioxide*, Geological Society London, Special Publications, 233, 181-191.
- Baines, S. J. and Worden, R.H. [2004] In: Baines S and Worden R.H. (Eds). *Geological storage of carbon dioxide*, Geological Society London, Special Publications, 233, 1-6.
- Benson, S., Hoversten, E., and Gasperikova, E. [2004] Overview of monitoring techniques and protocols for geologic storage projects. *IEA*

*Greenhouse Gas R&D Programme Report PH4/35*, 108pp.

- Carcione, J.M. and Helle, H.B. [1999] Numerical solution of the poro-viscoelastic wave equation on a staggered mesh. *J. Comput. Phys.* **154**(2), 520–527.
- Carcione, J.M., Helle, H.B., and Pham, N.H. [2003a]. White's model for wave propagation in partially saturated rocks: Comparison with poroelastic numerical experiments, *Geophysics*, **68**, 1389–1398.
- Carcione, J.M., Seriani, G., and Gei, D. [2003b] Acoustic and electromagnetic properties of soils saturated with salt water and NAPL, *J. Appl. Geophys.* **52**, 177–191.
- Carcione, J.M., Picotti, S., Gei, D. and Rossi, G. [2006] Physics and modelling for monitoring CO<sub>2</sub> Storage. *Pure Appl. Geophys.*, **163**, 175–207.
- Kikuta, K., Hongo, S., Tanase, D., and Ohsumi T. [2004] Field test of CO<sub>2</sub> injection in Nagaoka, Japan. In: M. Wilson, Morris, T., Gale, J., and Thambimuthu, K. (Eds.) *7<sup>th</sup> international conference Greenhouse Gas Control Technologies (GHGT-7) Vancouver, Canada*, Proceedings, 1367–1372.
- Kragh, E. and Christie, P. [2002]. Seismic repeatability, normalized rms and predictability. *The Leading Edge*, **21**, 642–647.
- Kreft, E. et al. [2006] Results of the second test program in K12-B, a site for Co<sub>2</sub> Storage and Enhanced Gas Recovery. *68<sup>th</sup> EAGE Conference, Vienna* (Expanded abstracts). D011.
- Morse, P.M. and Ingard, K.U. [1986]. *Theoretical acoustics*. Princeton University Press.
- Oldenburg, C.M. [2003]. Carbon Dioxide as Cushion Gas for Natural Gas Storage, *Energy & Fuels*, **17**, 240–246.
- Oldenburg, C.M., Stevens, S.H., and Benson, S.M. [2004]. Economic feasibility of carbon sequestration with enhanced gas recovery (CSEGR). *Energy*, **29**, 1413–1422.
- Polak, S. et al. [2006] The Atzbach-Schwanenstadt gas field - a potential site for onshore CO<sub>2</sub> storage and EGR. *The Leading Edge*, **25**, 1270–1275.
- Riddiford, F. I., Wight, C. Bishop, T., Espie, and Tourqui, A. [2004] Monitoring Geological Storage in the InSalah Gas CO<sub>2</sub> Storage Project. *Proceedings of the 7th International Conference on Greenhouse Gas Control Technologies (GHGT-7)*, Vancouver, Canada.
- Rossi, G., Gei, D., Böhm, G., Madrussani, G., and Carcione, J.M. [2007] Attenuation tomography: an application to gas-hydrate and free-gas detection, *Geophysical Prospecting*, **55**, 655–669.
- Sherlock, D., Toomey, A., Hoversten, M. Gasperikova, E., and Dodds, K. [2006] Gravity modelling of CO<sub>2</sub> storage in a depleted gas field: a sensitivity study. *Exploration Geophysics*, **37**, 37–43.
- Vesnaver, A. and Böhm, G. [2000] Staggered or adapted grids for seismic tomography? *The Leading Edge*, **19**, 944–950.
- Vesnaver, A., Böhm, G., Madrussani, G., Petersen, S., and Rossi, G. [1999] Tomographic imaging by reflected and refracted arrivals at the North Sea. *Geophysics*, **64**, 1852–1862.